JOURNAL OF PROPULSION AND POWER
Vol. 12, No. 4, July–August 1996

Effect of Heat Release on Streamwise Vorticity Enhanced Mixing

David S. Underwood* and Ian A. Waitz†
Massachusetts Institute of Technology, Cambridge, Massachusetts 02139

Experiments have been carried out to determine the effect of heat release on streamwise vorticity enhanced mixing of two coflowing streams. A lobed mixer and flat plate were examined in both reacting and nonreacting environments. Mixing rates were calculated by comparing experimental static pressure and mass-averaged total enthalpy measurements with the predictions of a quasi-one-dimensional control volume model in which a mixing rate could be specified. Initial mixing rates were shown to be increased by the introduction of streamwise vorticity, while the mixing rate augmentation because of the addition of streamwise vorticity was found to be less sensitive to the detrimental effects of heat release on mixing than the planar shear-layer mixing rate. The initial mixing rates obtained for the lobed mixer were greater than those for the flat plate by a factor of 6–12 for the different heat release cases. The mixing rate for the flat plate decreased by a factor of 4 for the highest heat release case compared with the zero-heat release case. This decrease was in agreement with the results of previous studies. The initial mixing rate downstream of the lobed mixer decreased by a factor of 2 from zero- to high-heat release, whereas the mixing rate far downstream of the trailing edge of the lobed mixer, after the streamwise vorticity had decayed, decreased by a factor of 3.6 from zero- to high-heat release. The skin friction losses over the lobed mixer were 7% of the average freestream dynamic head and were approximately five times greater than those over the flat plate. The mixing losses downstream of the trailing edge were greater for the lobed mixer than the flat plate, as expected, indicating more mixing with the lobed mixer.

I. Introduction

LOBED mixers are often employed to provide rapid, low-loss mixing between two coflowing fluid streams.[1–5] This increased mixing stems from two sources: 1) the increased trailing-edge length between the flat plate and the lobed mixer and 2) the cross-stream convection associated with the streamwise vorticity generated by the lobed mixer.[1,6]

The objective of the experiments described in this article was to quantify the effects of heat release on streamwise vorticity enhanced mixing. The experiments were conducted at the NASA Lewis Research Center. A flat plate and a lobed mixer were tested in reacting and nonreacting flows. Data included total temperature and total pressure surveys as well as wall static pressures. The data were used to determine the mixing rate via comparison of static pressure and mass flux weighted total enthalpy profiles obtained from the experiment with control volume results.

This article begins with a description of the experimental apparatus in Sec. II, followed by the test conditions in Sec. III, and the data acquisition procedures in Sec. IV. The control volume models used to determine mixing rates will then be presented in Sec. V. In Sec. VI the experimental results are discussed. Section VII contains a summary and conclusions.

II. Experimental Apparatus

The experiments were conducted in the NASA Lewis reacting shear flow facility. The test section was 20.3 cm wide, 10.2 cm high, and 63.5 cm long and exhausted to atmospheric pressure. Air was delivered at 820–920 K with a velocity of 170 m/s, whereas the fuel stream, composed of hydrogen and nitrogen, was delivered between 340–380 K with a velocity of 85 m/s (Ref. 7). The temperature nonuniformity at the inlet was less than 10 K. The upper and lower walls of the test section were hinged to adjust the axial pressure gradient. However, the maximum divergence angles were too small to maintain a zero axial pressure gradient during the runs, so the walls were set at a 1-deg divergence angle throughout the tests.

Schematics of the two geometries tested are shown in Fig. 1. The first was a flat plate with a convergence angle of 6.9 deg and trailing-edge thickness of 0.10 cm. The second was a lobed mixer with a penetration angle α of 22 deg, lobe wavelength λ of 2.54 cm, height-to-wavelength ratio h/λ of 1.25, and trailing-edge thickness of 0.10 cm. This geometry is typical of current lobed mixer technology.

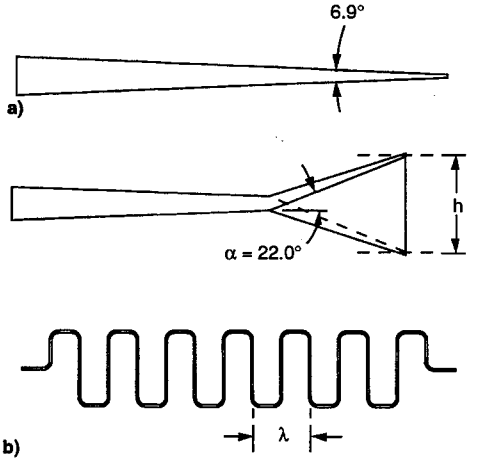

Fig. 1 Schematic of a) flat plate and b) lobed mixer (side- and trailing-edge views).

Presented as Paper 95-2471 at the AIAA/ASME/SAE/ASEE 31st Joint Propulsion Conference and Exhibit, San Diego, CA, July 10–12, 1995; received Sept. 11, 1995; revision received Feb. 18, 1996; accepted for publication Feb. 22, 1996.

*Graduate Research Assistant, Aero-Environmental Research Laboratory, Room 31-256. Student Member AIAA.

†Assistant Professor, Aeronautics and Astronautics, Aero-Environmental Research Laboratory, Room 31-268. Senior Member AIAA.

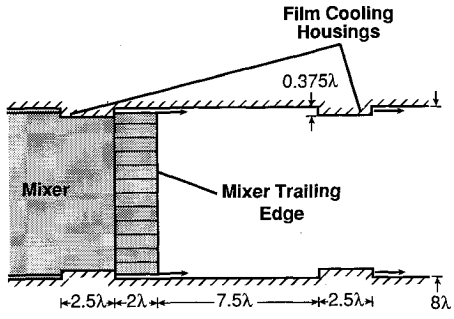

Fig. 2 Schematic of flow path in the test section. Flow is from left to right.

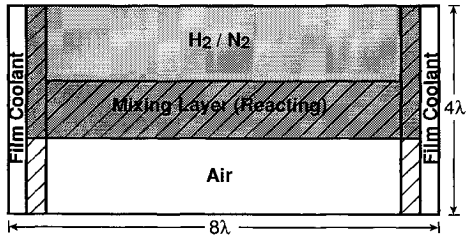

Fig. 3 Cross section of the flow in the test section, showing mixing and combustion zones.

Visual access to the flowfield was through two quartz windows. Total temperature and total pressure measurements were made with a water-cooled probe coated with a ceramic thermal barrier. The probe incorporated both a total pressure tube and a type R thermocouple.

Figure 2 shows the test section flow path with flow from left to right. The protrusions into the test section just upstream of the trailing edge of the mixer and then again at 7.5-lobe wavelengths downstream are housings for film cooling injection. Immediately downstream of the housings were the windows for which the cooling flow was provided. The film cooling gas was air.

The result of the cooling air injection is shown schematically in Fig. 3. The main mixing zone with combustion between the main fuel and airstreams is shown as the hashed, horizontal region in the center of the duct. There were also two mixing zones created between the film cooling air and each of the main streams, shown as the hashed vertical regions on the sides of the duct. The portion of the mixing layer between the film cooling air and the main fuel and combustion zones yielded additional heat release beyond that associated with the primary mixing/reaction zone. The effect of the additional mass injection and heat release due to the film cooling was accounted for when reducing the data and will be discussed in detail in Sec. V.B and Appendix A.

III. Test Conditions

The flat plate and lobed mixer were tested in both reacting and nonreacting flows. The nonreacting flow conditions consisted of nitrogen at 360 K in the low-speed stream and air at 820 K in the high-speed stream. The inlet velocities of the low- and high-speed streams were 85 and 170 m/s, respectively, yielding a velocity ratio $r = U_2/U_1$, between the two streams of 0.5, where U_2 is defined as the low-speed flow velocity and U_1 as the high-speed flow velocity.

Two reacting flow conditions were tested, corresponding to two different concentrations of hydrogen in the low-speed stream. Tests were run with $\Phi = 1.48$ in the low-heat release case and $\Phi = 1.84$ in the high-heat release case, where Φ is the equivalence ratio, defined as the ratio of the mass flow of hydrogen to oxygen at the inlet divided by this ratio at stoichiometric conditions. During reacting runs, the fuel stream was heated to 340 K and the airstream was heated to 920 K. The nominal velocity ratio between the two streams was 0.5 with the inlet velocities being the same as for the nonreacting runs. The tests were conducted with a Damköhler number of $Da \approx 5000$, where the Damköhler number is defined as the ratio of the residence time in the test section to the characteristic chemical reaction time. For complete mixing, the total enthalpy rise $\Delta h_t/h_{t,\text{inlet}}$ for the high-heat release case ($\Phi = 1.84$) was approximately 300%, in the range of practical interest for a gas turbine combustor. The total enthalpy rise for the low-heat release case ($\Phi = 1.48$) was approximately 200%.

IV. Data Acquisition

Planar total pressure and total temperature surveys were taken for each geometry at each of the three flow conditions described in Sec. III. These surveys were taken at distances of 1.2-, 2.5-, 5.2-, and 14.6-lobe wavelengths downstream of the trailing edge of the mixer. The flow was sampled with a single probe every 0.10-lobe wavelengths in a plane 3-lobe wavelengths high and 1.5-lobe wavelengths wide. Figure 4 shows a survey plane and its relation to the various regions of the flowfield shown in Fig. 3, whereas Fig. 5 shows the position of the four survey planes in relation to the trailing edge. The uncertainty in the total temperature measurements, after radiation, conduction, and catalytic corrections were made, was 10 K, whereas the uncertainty in the total pressure measurements was 276 Pa.

Static pressure data were taken at five points downstream of the trailing edge. Four of these points corresponded to the four survey planes mentioned previously. The fifth static tap was located at 4.0-lobe wavelengths downstream of the trailing edge. The uncertainty in the static pressure measurements was 138 Pa for all tests.

V. Data Analysis

The main objective of the experiments was to determine the mixing rate in the primary mixing layer shown in Fig. 3. However, the film coolant flows complicated this by producing additional reacting and nonreacting mixing zones. A quasi-one-dimensional control volume model was developed as a tool for determining the primary mixing rate at each test condition. Integration of the conservation equations for mass, momentum, and energy with a one-step mechanism for chemical reaction was carried out in the control volume model, allowing the specification of a single mixing rate between the two primary streams, while taking the film cooling zones into account. The primary stream mixing rate was iterated on until the static pressure and mass-averaged total enthalpy profiles given by the

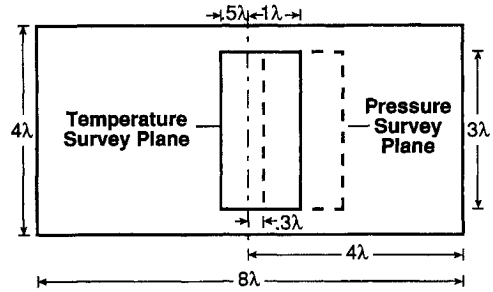

Fig. 4 Location of total temperature and total pressure survey planes in the duct. Flow is out of the page.

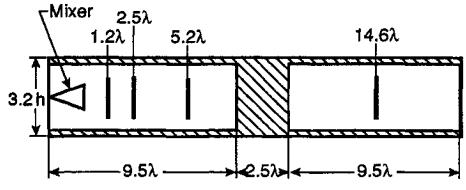

Fig. 5 Axial locations of survey planes.

control volume model agreed with those measured in the experiment. Before describing the complete model in Sec. V.B, a simplified model will be discussed in Sec. V.A to illustrate the basic data analysis technique.

A. Simplified Control Volume Model

The primary mixing zone was modeled as two streams with a growing shear layer between them, as depicted in Fig. 6. The mixing rate was specified by setting the amount of fluid entrained into the shear layer from the outer two streams. The ratio of mass entrainment from the high- and low-speed streams was computed using the relation given by Hermanson and Dimotakis, which accounted for variations in the free-stream density and velocity ratios.[8] The total entrainment was varied until the static pressure and total enthalpy profiles agreed with those obtained from the experiment.

The analysis employed the simplified reaction mechanism

$$\left(H_2 + \frac{1}{\alpha} N_2\right) + \frac{1}{2\psi}(O_2 + 3.76N_2) \rightarrow H_2O + \left(\frac{1}{2\psi} - \frac{1}{2}\right) O_2 + \left(\frac{1.88}{\psi} + \frac{1}{\alpha}\right) N_2 \quad (1)$$

where α is the ratio of moles of hydrogen to moles of nitrogen in the fuel stream, and ψ is the equivalence ratio Φ, defined previously, multiplied by the ratio of the number of moles of hydrogen to oxygen being entrained into the shear layer at every downstream location. Since the Damköhler number was approximately 5000, it was assumed that all reactants entrained into the shear layer combusted completely and instantaneously. It was also assumed that the pressure was uniform in any given plane downstream of the trailing edge.

The assumption of uniform static pressure was evaluated using a three-dimensional Reynolds-averaged, Navier–Stokes code.[9] A numerical simulation of the lobed mixer flow was performed for nonreacting flow with a velocity ratio r of 0.5, α of 22 deg, and h/λ of 1.0. The lowest and highest static pressure coefficients, $C_p = \Delta p/\bar{q}$ (where $\bar{q}$ is the average inlet dynamic head $\bar{\rho}\bar{u}^2/2$) in a plane, were compared to the mass-averaged C_p and found to deviate by less than ± 0.1 near the trailing edge. After four wavelengths downstream, the deviation was less than ± 0.01. Thus, the static pressure nonuniformities were small in the near field of the mixer and negligible in the far field, and the assumption of uniform static pressure was justified. An order of magnitude estimate was also made for the variation in static pressure caused by turbulent fluctuations, which was not accounted for in the conservation equations. Based on the relations of Brown and Roshko,[10] the magnitude of these fluctuations was found to be 0.25% of the inlet dynamic head for the flat plate and 1.4% for the lobed mixer.

B. Complete Control Volume Model

As noted in Sec. II, there was mixing between the main streams and the film cooling air as well as combustion caused by part of this mixing. There were also changes in duct area caused from the film cooling housings and wall divergence. A more complete control volume model, shown in Fig. 7, was developed to account for these effects.

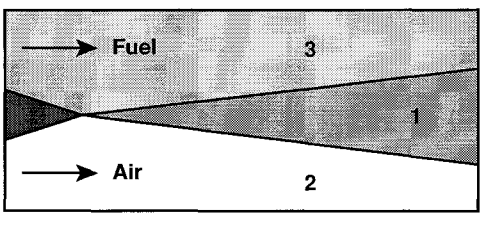

Fig. 6 Simplified, three-stream control volume model. Flow is from left to right.

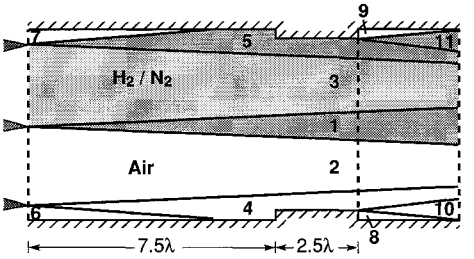

Fig. 7 Complete, 11-stream control volume model.

The main inflow streams and shear layer were denoted by streams 1, 2, and 3. These three streams composed the simplified model discussed in Sec. V.A. Two film cooling streams were injected on the top and bottom, shown as streams 6 and 7. These streams entered with different velocities than the main streams. The shear layer between the fuel stream and the top film cooling stream (stream 5) combusted, while the bottom shear layer (stream 4) did not. At $x/\lambda = 7.5$, a step change in the duct area occurred where the second film cooling housing began. Another 2.5 wavelengths downstream of this, the second mass injection occurred. There was reaction in the shear layer labeled stream 11, whereas no reaction occurred in the bottom shear layer, stream 10.

The corrections associated with the film cooling flows were small compared to the overall trends measured. The mixing rates for the film cooling shear layers were specified based on results from experimental calibration tests as described in Appendix A. Then the main mixing rate for stream 1 was changed until the predicted static pressure and mass-averaged total enthalpy profiles matched the experimental static pressure and mass-averaged total enthalpy profiles. The criteria adopted for determining the best match was that the computed static pressure be within $\pm 5\%$ of the experimental value for no less than four of the five measurement points. The criteria adopted for matching the total enthalpy was that the computed total enthalpy be within $\pm 5\%$ of the experimental value for no less than three of the four measurement points. These criteria were used throughout for all static pressure and total enthalpy matching.

VI. Results

Total temperature surveys are presented in Sec. VI.A., followed by the mass-averaged total enthalpy and static pressure data in Sec. VI.B. In Sec. VI.C, the mixing rates derived from the experimental data using the control volume model will be presented and discussed, while the results for the effect of heat release on the mixing augmentation because of streamwise vorticity will be presented in Sec. VI.D. Section VI.E presents a comparison of the total pressure losses for the flat plate and lobed mixer.

A. Total Temperature Surveys

Figure 8 shows total temperature surveys for the lobed mixer with high-heat release at the first three downstream locations. The fuel stream is the upper stream, and a trace of the lobed mixer trailing edge has been overlayed on the plots. The overall flow structure shown is typical of results obtained for nonreacting lobed mixer flows.[1,2,7] At $x/\lambda = 1.2$, the mixing interface has begun to roll up, showing the influence of the shed streamwise vorticity. At $x/\lambda = 2.5$, the interface has rolled up enough to pinch off the bottom of the fuel region (the dark blue area in the region $-0.5 < y/\lambda < -0.1$). By the next downstream location, $x/\lambda = 5.2$, significant mixing and reaction have occurred, and the temperature profile is more uniform, similar to that of a planar shear layer.

B. Static Pressure and Total Enthalpy Profiles

Figures 9 and 10 show experimental static pressure C_p and mass-averaged total enthalpy C_{ht} measurements. The lines rep-

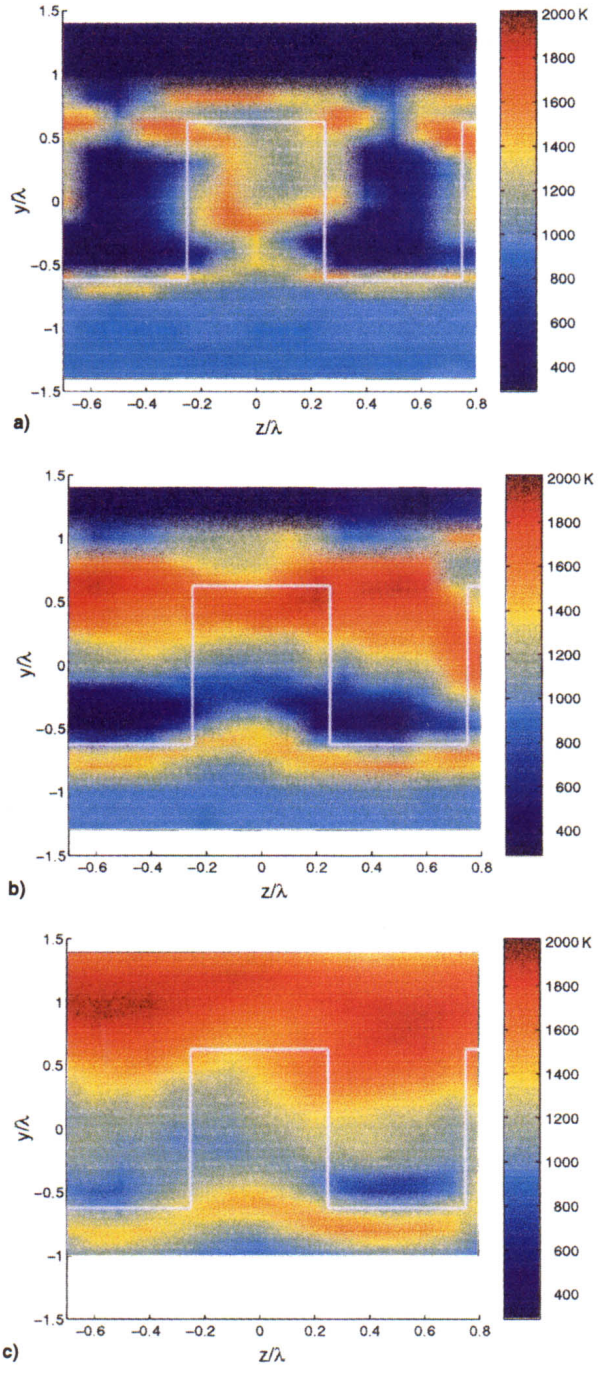

Fig. 8 Total temperature contours for the lobed mixer with high-heat release at the first three survey planes. x/λ = a) 1.2, b) 2.5, and c) 5.2.

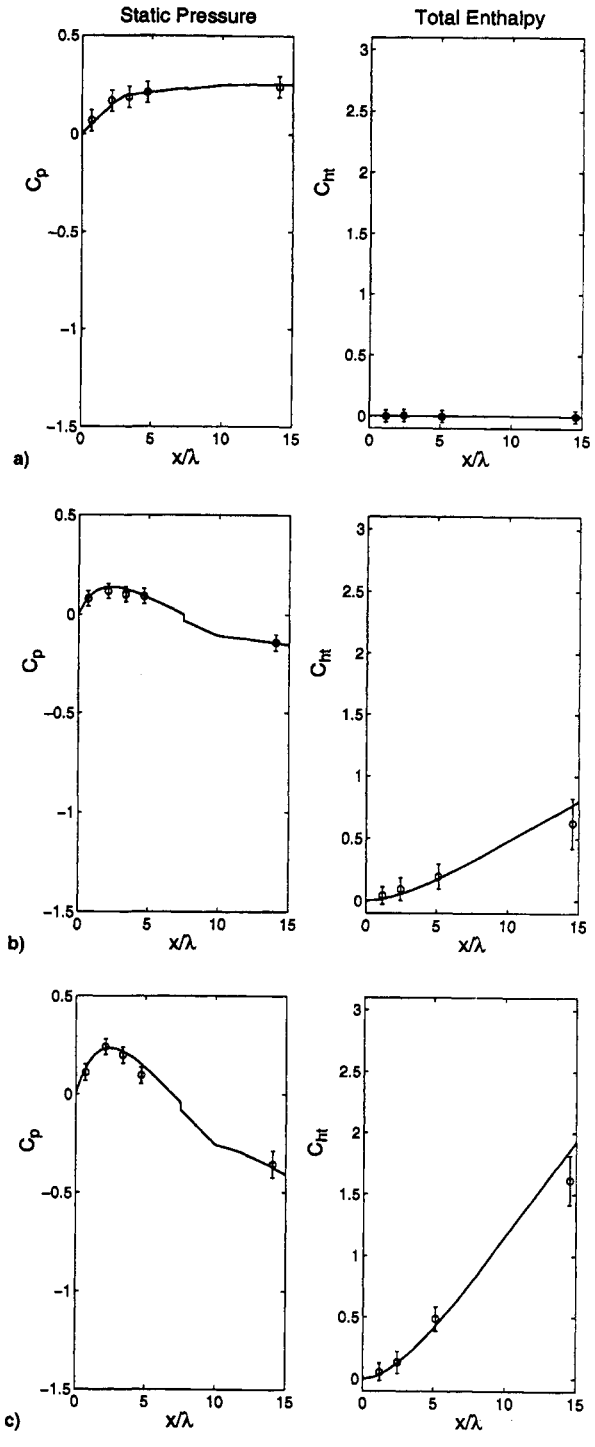

Fig. 9 Flat plate experimental (○) and computed (line) static pressure and total enthalpy profiles for Φ = a) 0, b) 1.48, and c) 1.84.

resent the results of the control volume model discussed in Sec. V.B. The static pressure has been matched to the experimental data by adjusting the primary mixing rate. The static pressure rise coefficient $C_p = \Delta p/(\bar{\rho}\bar{u}^2/2)$, is defined as before. The total enthalpy rise coefficient is defined as $C_{ht} = \Delta\bar{h}_t/\bar{h}_{t,\text{inlet}}$. The error bars shown in Figs. 9 and 10 were obtained by estimating the random and bias errors in each of the measured quantities. The errors were then propagated through the calculation of C_p and C_{ht} and plotted as 95% confidence bands.

Comparison of Figs. 9a and 10a shows that for zero-heat release, the static pressure rise for the lobed mixer was almost double that of the flat plate. This result is typical of flows generated by lobed mixers with the geometry described in Sec. II.[2] Comparing Figs. 9a and 10a with Figs. 9c and 10c, it is evident that the addition of heat release changed the static pressure profiles markedly. Although a pressure rise because of mixing still existed, the pressure drop because of the combustion process more than counteracted this, yielding a net reduction in pressure. The exit pressure coefficient for the lobed mixer varied from +0.45 with zero-heat release to −1.05 with high-heat release. Also notice that, as expected, the enthalpy rise increased as Φ increased.

Comparison of Figs. 9b and 10b shows that for the low-heat release case (Φ = 1.48), the mixing augmentation because of the lobed mixer produced almost four times the pressure drop produced by the flat plate, and the enthalpy rise was more than double. This effect is seen again in Figs. 9c and 10c for the high-heat release case (Φ = 1.84), where the pressure drop was

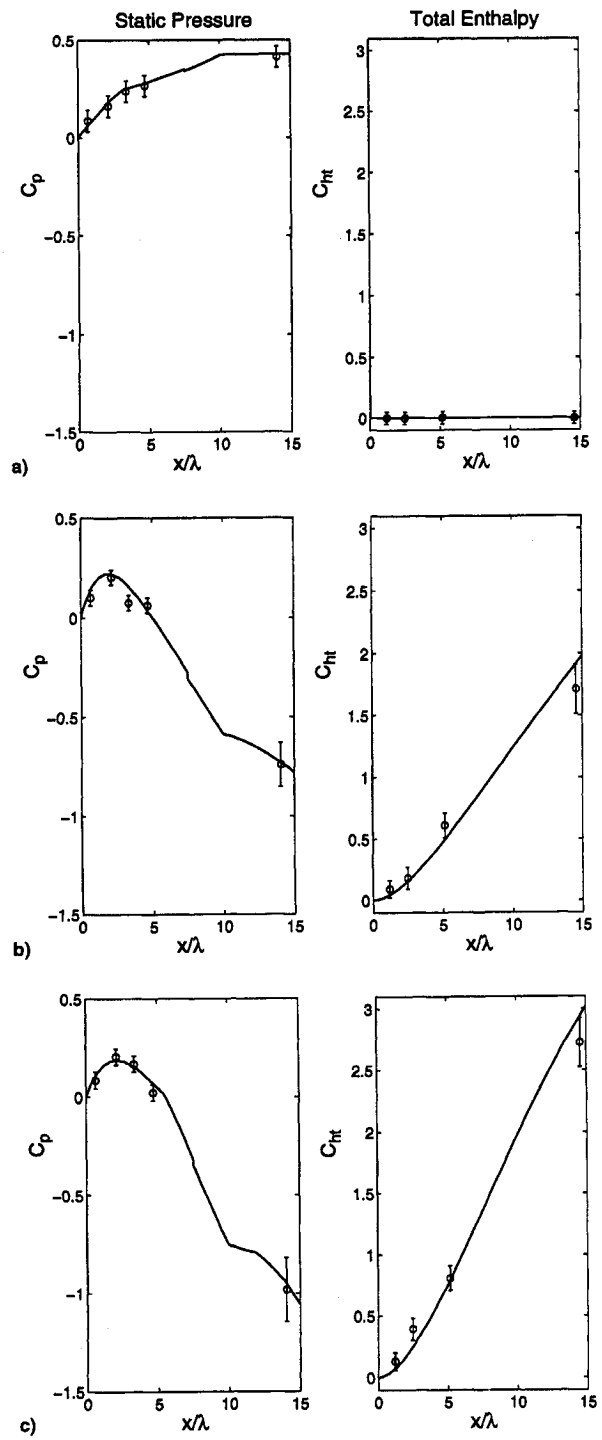

Fig. 10 Lobed mixer experimental (○) and computed (line) static pressure and total enthalpy profiles for Φ = a) 0, b) 1.48, and c) 1.84.

increased by a factor of 2.5, and the enthalpy rise was increased by a factor of 1.5.

The sensitivity of the derived mixing rate to changes in static pressure or mass-averaged total enthalpy was also examined.[7] Mixing rate was varied in the control volume model to match either static pressure or total enthalpy to the upper and lower points of the error bars shown in Figs. 9 and 10. For all of the experimental cases, the change in mixing rate was greater when static pressure, not mass-averaged total enthalpy, was matched at the high and low points of the error bars. Thus, the mixing rate determination was more sensitive to static pressure than total enthalpy. Therefore, throughout this study, static pressure was matched to determine mixing rate.

C. Mixing Rates and Mixedness

Scalar mixedness was used as a measure of species transport. This mixedness parameter is defined as

$$M = \dot{m}_{\text{mix}}/\dot{m}_{\text{in}} \tag{2}$$

where $\dot{m}_{\text{mix}}$ is the mass flow rate of products in the mixing layer, and $\dot{m}_{\text{in}}$ is the mass flow rate of reactants in the experimental survey plane ($-1.5 < y/\lambda < 1.5$ and $-0.7 < z/\lambda < 0.8$) at the inlet. The value of M can vary from 0 at the trailing edge, representing two completely unmixed fluid streams, to 1 far downstream, representing two completely mixed fluid streams. No film cooling air was present in the surveyed regions, therefore, the film cooling mass flow rate was not included in the calculation of $\dot{m}_{\text{in}}$. Because of the assumption in the control volume model that all fluid entrained into the shear layer is combusted completely and instantaneously, the mixedness parameter reflects only that fluid which has been molecularly mixed.

The effect of heat release on mixedness is shown in Fig. 11. The shaded areas represent the effect on the calculated mixedness if the static pressure profiles were matched through the upper and the lower points of the experimental error bars as discussed earlier in Sec. VI.B. The line in the middle of each shaded region is the best estimate of the mixing rate. This being the mixing rate that produced the static pressure profiles shown in Figs. 9 and 10. From Fig. 11, the mixing rate, given by the slope of the mixedness curve, can be seen to decrease with increasing heat release.

As shown in Fig. 11a the flat plate mixing rate decreased by a factor of 4 for the high-heat release case (Φ = 1.84)

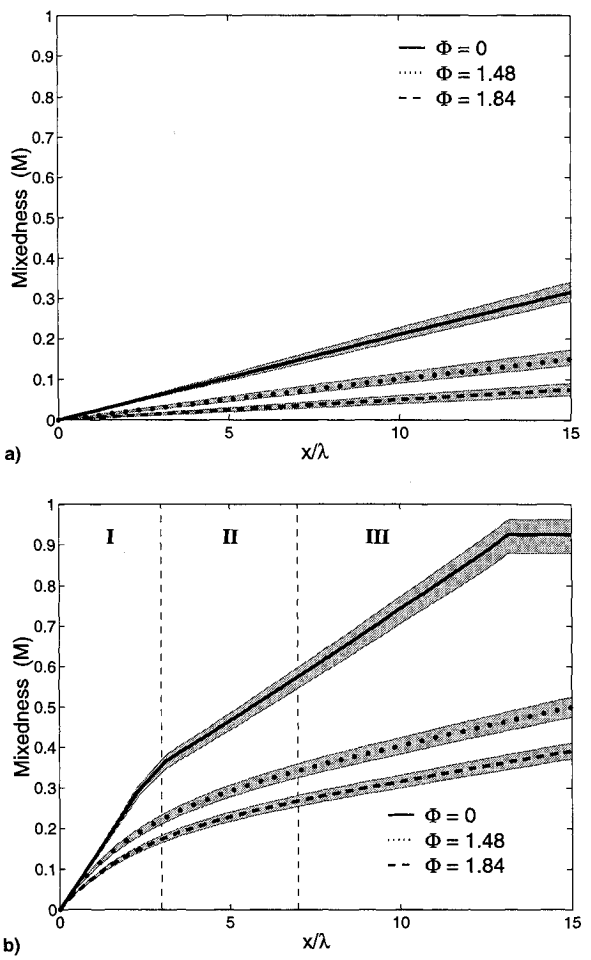

Fig. 11 Mixedness curves with error bands for the a) flat plate and b) lobed mixer.

Table 1 Comparison of flat plate mixing rates for varying heat release with the results of Hermanson and Dimotakis[8]

Heat release, Φ	Present study	Hermanson and Dimotakis[8]
0	0.021	0.019
1.48	0.010	0.009
1.84	0.005	0.006

compared to the flat plate mixing rate for the zero-heat release case. Comparing Figs. 11a and 11b, it can also be seen that the lobed mixer initially mixed approximately six times faster than the flat plate at zero-heat release and approximately 12 times faster at high-heat release. The initial mixing rate for the lobed mixer was decreased by a factor of 2 from zero- to high-heat release, whereas the mixing rate in the far field of the lobed mixer for the high-heat release case was decreased by a factor of 3.6 compared to the zero-heat release case. Thus, in the near field of the lobed mixer ($x/\lambda \leq 3$), the mixing rate was less sensitive than that of the flat plate flow to the detrimental effects of heat release.

The higher mixing rate for the lobed mixer increased the level of mixedness at the last survey plane for the zero-heat release case by a factor of 3 over the flat plate mixedness at zero heat release, while the final mixedness for the lobed mixer at high-heat release was greater than that of the flat plate at high-heat release by a factor of 5. The mixedness of the lobed mixer flow at the last measurement plane was decreased by a factor of 2.3 for the high-heat release case compared to the lobed mixer with zero-heat release. Note that the change in the lobed mixer mixing rate with heat release in the far field was approximately proportional to the change in the flat plate mixing rate.

Table 1 compares the mixing rates for the flat plate at zero-, low-, and high-heat releases as shown in Fig. 11a with the results of Hermanson and Dimotakis[8] for a flat plate with the same heat releases. The results for the flat plate agree within 10% with those of Hermanson and Dimotakis.

It is important to determine whether the measurements taken near the trailing edge were in a region dominated by the trailing-edge wake. The results of an analysis to determine this are presented in Appendix B. These results support the assumption that the trailing-edge wake effects were small.

A virtual origin for the shear layer was not included in the analysis as it had little effect on the derived mixing rate. The virtual origin x_0/λ was determined by examining the total temperature data and was found to vary from -0.050 for zero-heat release to -0.088 for high-heat release. Neglecting the virtual origin caused a maximum error in the flat plate mixing rate of 2.0% for zero-heat release and 3.4% for high-heat release. This error falls within the error bands on the mixedness curves.

D. Mixing Augmentation with Heat Release

The lobed mixer had three regions where the mixing behavior was different. Figure 11b shows these regions. In region I, streamwise vorticity had a dominant effect. In region III, comparison with numerical simulations and the cold-flow experiments of McCormick suggests that the streamwise vorticity had decayed, and was no longer having a strong influence on the mixing process.[1,6] In region II, the behavior was some combination of these two cases.

The focus will first be on region I where streamwise vorticity had a dominant effect. Two contributions to mixing rate were identified and evaluated for the lobed mixer flow. The first was the increased mixing interface length caused by the increased trailing-edge length of the lobed mixer. This will be called the interface-scaled planar shear-layer mixing rate, and will be denoted as $l\mathrm{d}M_{\mathrm{psl}}$, where l is the lobed mixer to flat plate trailing-edge length ratio, and $\mathrm{d}M_{\mathrm{psl}}$ is the planar shear-layer mixing rate with the denominator $\mathrm{d}(x/\lambda)$, dropped for convenience, but implied. The second contribution was the additional mixing associated with the shed streamwise vorticity. This increase in mixing rate will be denoted by $\mathrm{d}M_a$ and will be called the augmented mixing rate. Thus, the overall mixing rate of the lobed mixer is given by

$$\mathrm{d}M_{\mathrm{tot}} = \mathrm{d}M_a + l\mathrm{d}M_{\mathrm{psl}} \tag{3}$$

where $\mathrm{d}M_{\mathrm{tot}}$ is the slope of the lobed mixer mixedness curves shown in Fig. 11b.

The experimental mixing augmentation rates were found by subtracting the interface-scaled planar shear-layer mixing rate $l\mathrm{d}M_{\mathrm{psl}}$, from the total mixing rate $\mathrm{d}M_{\mathrm{tot}}$, as suggested in Eq. (3). For these experiments, $l = 3.2$. The values for the initial lobed mixer mixing rates were calculated by averaging the slope of the mixedness curves over the first three wavelengths. This distance was used based on the results of Fung and McCormick.[1,6,7]

Table 2 shows the values of the overall mixing rates observed for a flat plate and lobed mixer, while Table 3 shows the derived values for the augmented mixing rate. These results show that the mixing augmentation due to streamwise vorticity was reduced approximately 18% by heat release. This reduction may be compared to the 76% reduction displayed in the flat plate data shown in Fig. 11a. Therefore, the results show that heat release reduces the molecular mixing caused by streamwise vorticity. Because only molecularly mixed fluid was considered in the calculation of mixedness and mixing rate, it is not possible to say whether this is because of a decrease in the entrainment of freestream fluid or a decrease in the fine-scale mixing.

The effect of a large favorable pressure gradient on mixing rate was examined by accounting for the mixing rate augmentation associated with axial stretching of the shear layer based on scalings presented by Karagozian and Marble.[11] This effect produced less than a 2% increase in the observed mixing rate for the flat plate and lobed mixer at all heat releases. Therefore, the effect of the large favorable pressure gradient on mixing rate was small.

E. Total Pressure Losses

There are two primary sources of total pressure loss in lobed mixer and flat plate flows. The first is the skin friction loss over the lobes or flat plate. The second is the loss caused by the mixing out of velocity nonuniformities downstream of the trailing edge.

The skin friction losses over the lobed mixer and flat plate were evaluated using the total pressure and total temperature

Table 2 Flat plate and lobed mixer mixing rates

Heat release, Φ	$\mathrm{d}M_{\mathrm{psl}}$	$l\mathrm{d}M_{\mathrm{psl}}$	$\mathrm{d}M_{\mathrm{tot}}$
0	0.021	0.067	0.117
1.48	0.010	0.032	0.073
1.84	0.005	0.016	0.057

Table 3 Observed mixing augmentation rates

Heat release, Φ	$\mathrm{d}M_a$
0	0.050
1.48	0.041
1.84	0.041

Table 4 Experimental and computational loss coefficients L for flow over the lobed mixer and flat plate

Geometry	Experimental	Computational
Flat plate	0.015	0.014
Lobed mixer	0.070	0.070

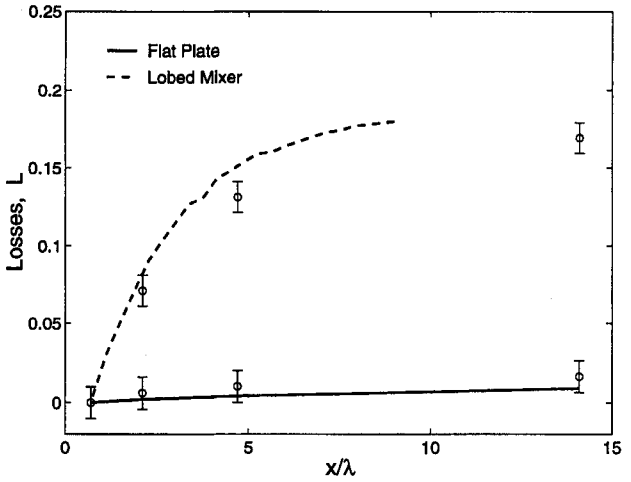

Fig. 12 Experimental (○) and computational (line) loss coefficients for flow downstream of the lobed mixer and flat plate.

surveys as well as the wall static pressure measurements. The loss coefficient L is defined as

$$L = \frac{\bar{p}_{t,\text{in}} - \bar{p}_t}{\bar{q}_{\text{in}}} \tag{4}$$

where $\bar{p}_{t,\text{in}}$ is the mass-averaged total pressure at the beginning of the lobes or flat plate, $\bar{p}_t$ is the mass-averaged total pressure at the trailing edge, and $\bar{q}_{\text{in}}$ is the average dynamic pressure at the entrance to the lobes. The results of this comparison are shown in Table 4. The skin friction losses over the lobed mixer were 7% of the average dynamic head and were approximately five times greater than those over the flat plate. These loss coefficients compare well with the results of the three-dimensional Navier–Stokes simulation described in Sec. V.A.

The losses for the flat plate and lobed mixer downstream of the trailing edge were also obtained from the experimental measurements. The loss coefficient is defined as before in Eq. (4) where $\bar{p}_{t,\text{in}}$ is the mass-averaged total pressure at the trailing edge, $\bar{p}_t$ is the mass-averaged total pressure at a given downstream location, and $\bar{q}_{\text{in}}$ is the average dynamic pressure at the trailing edge. The results of this comparison are shown in Fig. 12. The circles represent the experimental data and the lines represent the results of the Navier–Stokes code. These results show that the mixing losses are greater for the lobed mixer than the flat plate, as expected, indicating more mixing for the lobed mixer. The agreement between the results of the Navier–Stokes code and the experiments for the flat plate is good. The code overestimated the losses for the lobed mixer by approximately 25%. This coincided with an initial mixing rate that was approximately 25% higher for the computational results.

VII. Conclusions

A lobed mixer and flat plate were tested in both reacting and nonreacting environments. The mixing rates were calculated by comparing experimental static pressure and mass-averaged total enthalpy profiles with the predictions of a quasi-one-dimensional control volume model. The control volume model performed well, giving insights into the behavior of state variables and allowing determination of mixing rates with a small computational effort (approximately 1 min on an IBM RS6000 workstation).

The conclusions of this study are as follows:

1) Mixing augmentation occurred when streamwise vorticity was added to a reacting flow using a lobed mixer. The initial mixing rate of the lobed mixer was greater than the flat plate mixing rate by a factor of 6–12 for the different heat release cases.

2) The augmented mixing rate in the near field of the lobed mixer was found to be less sensitive to the detrimental effects of heat release than the planar shear-layer mixing rate. The planar shear-layer mixing rate dM_{psl} was decreased by 76% from zero- to high-heat release, whereas the overall mixing rate for the lobed mixer was decreased by 51%, with the contribution associated with the streamwise vorticity decreasing by only 18%.

3) The decrease in mixing rate with increasing heat release for a flat plate compared well with the results presented by Hermanson and Dimotakis.[8]

4) The mixing rate associated with a lobed mixer was found to decrease with increasing heat release after the streamwise vorticity had decayed. The decay in mixing rate with heat release in the far field was approximately proportional to the decay in mixing rate observed for the flat plate.

5) The skin friction and mixing losses were greater for the lobed mixer than the flat plate. The skin friction losses over the lobed mixer were 7% of the average dynamic head and were approximately five times greater for the lobed mixer than the flat plate. The mixing losses downstream of the trailing edge were greater for the lobed mixer than the flat plate, indicating more mixing with the lobed mixer.

Appendix A: Film Cooling Mixing Rates

Film cooling mixing rates were determined by using the simplified control volume model with no reaction to model the mixing of one film cooling layer. Figure A1 shows the model used. The static pressure profile given by the simplified model was compared to experimental calibration data with varying film cooling flow rates. Effects because of mixing of the two primary inflow streams were minimized since these calibration tests were run with a flat plate at a velocity ratio of 1 and zero-heat release. At these conditions, pressure changes were due solely to changes in duct area and mixing between the film cooling air and the main airstreams.

A single film cooling mixing rate was specified so that the experimental and computed static pressure profiles agreed. This mixing rate was used for the two nonreacting film cooling shear layers, streams 4 and 10 as shown in Fig. 7. Figure A2 shows the best match between static pressure profiles for two film cooling flow rates.

The calibration tests could only be carried out for nonreacting conditions. The mixing rates for the two reacting film cooling shear layers were determined by scaling the cold flow mixing rates using the empirically derived scaling law of Hermanson and Dimotakis[8] for the entrainment of fluid into a

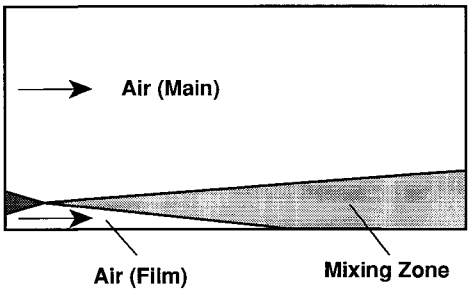

Fig. A1 Control volume model used for film cooling mixing rate determination.

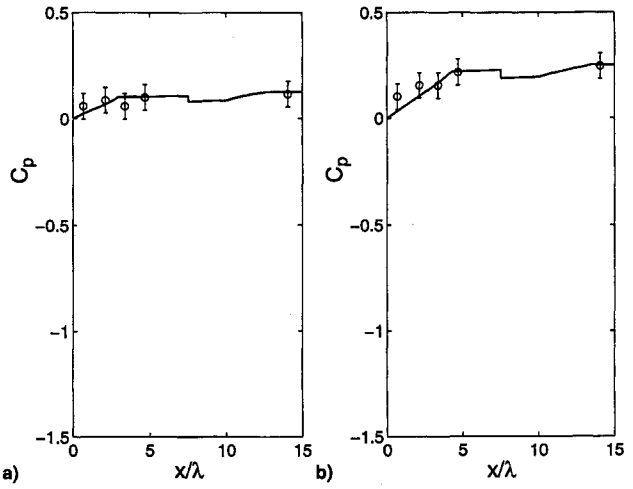

Fig. A2 Experimental (○) and computational (line) static pressure profiles. Film cooling mass flows of $\dot{m}_{film}/\dot{m}_{inlet}$ = a) 0.08 and b) 0.25.

reacting shear layer. Hermanson and Dimotakis have shown that the entrainment of fluid into a shear layer decreases with increasing heat release. Their data for a flat plate with varying heat release were used to determine the relative reduction in mixing rate at the heat releases encountered in the current experiments. This mixing rate was then used for the two reacting film cooling shear layers, streams 5 and 11 in Fig. 7. The mixing rates for streams 4, 5, 10, and 11 were left constant at these computed values during the final iteration on the main mixing rate in stream 1.

Comparison of the static pressure changes associated with the film cooling flow, shown in Fig. A1, with those associated with the main mixing process (see Figs. 9 and 10), shows that the relative effect of the film cooling was small compared to the trends measured. The pressure rise because of film cooling injection was approximately 10% of the pressure rise for the flat plate with no heat release. This dropped to 2.5% of the pressure rise for the lobed mixer with high-heat release.

Appendix B: Evaluation of Wake Effects

Hermanson has suggested that to ensure that there are no trailing-edge wake effects and to ensure that the mixing layer is self-similar, measurements in planar shear layers should be taken at least 1000 momentum thicknesses downstream of the trailing edge.[12] It is also desirable to be above the Reynolds number for mixing transition to ensure a turbulent mixing layer. In these tests, the Reynolds number based on the average freestream velocity and the downstream distance was typically 710,000. This was well above the Reynolds number for mixing transition as reported by Konrad.[13]

The momentum thickness at the trailing edge of both the flat plate and lobed mixer were computed. The flat plate boundary-layer thickness was found to be 3 mm, yielding a momentum thickness of 0.375 mm. The lobed mixer boundary-layer thickness was found to vary between 0.2–1.9 mm, yielding an average boundary-layer thickness of 1.05 mm. Based on this, the momentum thickness for the lobed mixer was found to be 0.13 mm, or 0.4% of the lobe height.

The flat plate boundary layer corresponded to 68 momentum thicknesses per lobe wavelength, while the average lobed mixer boundary layer was thinner at 195 momentum thicknesses per lobe wavelength. Thus, measurements were taken upstream of the 1000 momentum thickness guideline suggested by Hermanson.[12] However, the mixing rate data in Fig. 11a show that the planar shear layer displayed a linear growth rate for $x/\lambda \leq 1$. This implies that at the first measurement plane $x/\lambda = 1.2$ the flow behavior was similar to a fully developed turbulent shear layer. Since the lobed mixer had almost three times the number of momentum thicknesses per lobe wavelength as the flat plate, it was assumed that the mixing region downstream of the lobed mixer was also turbulent and fully developed.

Acknowledgments

Support for this work was provided by the NASA Lewis Research Center under NASA Grant NCC3-307 with C. Chang as Technical Monitor. This support is gratefully acknowledged. The authors would like to acknowledge E. M. Greitzer of the Massachusetts Institute of Technology and F. E. Marble of the California Institute of Technology for their many stimulating discussions and insightful suggestions. In addition, the authors would like to acknowledge J. Hermanson of the Worcester Polytechnic Institute for his valuable advice on the details of planar reacting shear layers; P. Lewis, formerly of the Massachusetts Institute of Technology, for his insights on combustion processes; J. Swan of the NASA Lewis Research Center for his assistance in the scheduling of test time; C. Wey of the NASA Lewis Research Center for his many insights and help in data collection; and A. Shott, G. Dutt, and B. Kirchner of the NASA Lewis Research Center for their help in maintaining and operating the reacting shear flow facility.

References

[1]McCormick, D. C., "Vortical and Turbulent Structure of Planar and Lobed Mixer Free-Shear Layers," Ph.D. Dissertation, Univ. of Connecticut, Storrs, CT, 1992.

[2]Manning, T. A., "Experimental Study of Mixing Flows with Streamwise Vorticity," M.S. Thesis, Massachusetts Inst. of Technology, Cambridge, MA, 1991.

[3]Qiu, Y. J., "A Study of Streamwise Vortex Enhanced Mixing in Lobed Mixer Devices," Ph.D. Dissertation, Massachusetts Inst. of Technology, Cambridge, MA, 1992.

[4]Seiner, J. M., and Krejsa, E. A., "Supersonic Jet Noise and the High Speed Civil Transport," AIAA Paper 89-2358, July 1989.

[5]McVey, J. B., and Peschke, W. T., "Study of Streamwise Vorticity-Stirred Combustion," United Technologies Research Center Rept. R93-958160-1, Dec. 1993.

[6]Fung, A. K. S., "Modeling of Mixer-Ejector Nozzle Flows," M.S. Thesis, Massachusetts Inst. of Technology, Cambridge, MA, 1995.

[7]Underwood, D. S., "Effects of Heat Release on Streamwise Vorticity Enhanced Mixing," M.S. Thesis, Massachusetts Inst. of Technology, Cambridge, MA, 1995.

[8]Hermanson, J. C., and Dimotakis, P. E., "Effects of Heat Release in a Turbulent, Reacting Shear Layer," *Journal of Fluid Mechanics*, Vol. 199, Feb. 1989, pp. 333–375.

[9]Krasnodebski, J., private communication, Aero-Environmental Research Lab., Massachusetts Inst. of Technology, Cambridge, MA, 1995.

[10]Brown, G. L., and Roshko, A., "On Density Effects and Large Structure in Turbulent Mixing Layers," *Journal of Fluid Mechanics*, Vol. 64, Pt. 4, 1974, pp. 775–816.

[11]Karagozian, A. R., and Marble, F. E., "Study of a Diffusion Flame in a Stretched Vortex," *Combustion Science and Technology*, Vol. 45, Nos. 1,2, 1986, pp. 65–84.

[12]Hermanson, J. C., "Heat Release Effects in a Turbulent, Reacting Shear Layer," Ph.D. Dissertation, California Inst. of Technology, Pasadena, CA, 1985.

[13]Konrad, J. H., "An Experimental Investigation of Mixing in Two Dimensional Shear Flows with Application to Diffusion Limited Chemical Reactions," Ph.D. Dissertation, California Inst. of Technology, Pasadena, CA, 1976.